

## FURTHER EVIDENCE FOR A WEAK NEUTRON STAR MAGNETOSPHERE IN THE ACCRETING MILLISECOND X-RAY PULSAR HETE J1900.1-2455

A. PATRUNO<sup>1,2</sup> & R. WIJNANDS<sup>3</sup>  
Draft version October 5, 2018

### ABSTRACT

HETE J1900.1–2455 is a peculiar accreting millisecond X-ray pulsar (AMXP) because it has shown intermittent pulsations after 22 days from the beginning of its outburst. The origin of intermittent pulses in accreting systems remains to be understood. To better investigate the phenomenon of intermittent pulsations here we present an analysis of 7 years of X-ray data collected with the *Rossi X-Ray Timing Explorer* and focus on the aperiodic variability. We show that the power spectral components follow the same frequency correlations as the non-pulsating atoll sources. We also study the known kHz QPO and we show that it reaches a frequency of up to  $\approx 900$  Hz, which is the highest frequency observed for any kHz QPO in an AMXP. We also report the discovery of a new kHz QPO at  $\approx 500$  Hz. Finally, we discuss in further detail the known pulse phase drift observed in this source, which so far has no explanation. We interpret the behavior of the aperiodic variability, the high frequency of the 900 kHz QPO and the presence of the pulse drift as three independent pieces of evidence for a very weak neutron star magnetosphere in HETE J1900.1–2455.

*Keywords:* pulsars: individual HETE J1900.1-2455 – X-Rays: binaries – X-Rays: accretion

### 1. INTRODUCTION

The accreting millisecond X-ray pulsar (AMXP) HETE J1900.1–2455 (henceforth referred to as J1900) is a binary with an orbital period of 1.4 hr composed by a neutron star spinning with a frequency of about 377 Hz and a  $0.02 M_{\odot}$  brown dwarf. This source is a very peculiar one among the AMXP family (see e.g., [Patruno & Watts 2012](#) for a review on AMXPs). J1900 is a quasi-persistent source (i.e., showing years-long outbursts) whose first outburst was detected on June 14, 2005 by the *High Energy Transient Explorer-2* ([Vanderspek et al. 2005](#)) and its outburst has lasted for approximately 10 years ([Degenaar et al. 2017](#)). Two days after its discovery, observations taken with the *Rossi X-ray Timing Explorer* (*RXTE*) showed X-ray pulsations ([Kaaret et al. 2006](#)). The pulsations have a unique and peculiar behavior as they were first continuously detected for approximately 22 days ([Kaaret et al. 2006](#)), then they became intermittent ([Galloway et al. 2007, 2008a](#)) appearing and disappearing on a timescale of a few days. After a few tens of days the pulsations became extremely intermittent, appearing sporadically at very low amplitudes for the next 2 years ([Patruno 2012](#)) and finally they became undetectable with upper limits of  $\lesssim 0.5 - 0.1\%$  rms on the pulsed amplitudes for the remaining time until December 5th, 2011, when *RXTE* stopped monitoring the source. A simultaneous *RXTE* and *XMM-Newton* observation performed on September 19–20, 2011 also revealed no pulsations down to 0.4% amplitude ([Papitto et al. 2013](#)).

[Kaaret et al. \(2006\)](#) reported the appearance of a 882 Hz Quasi-Periodic-Oscillation (the so-called kHz QPO) in coincidence with a relatively large flare in the X-ray lightcurve of J1900, occurring about 22 days after the beginning of the monitoring campaign. As noted by [Galloway et al. \(2007\)](#), pulse intermittency sets in right after this flaring episode.

[Patruno \(2012\)](#) also found a very large pulse phase shift ( $\approx -0.7$  cycles) in coincidence with the flare. The pulse phases drifted roughly constantly for  $\approx 3000$  seconds, until they reached a phase of  $\phi \approx -0.1$  cycles towards the end of the observation. Whether the flare, the kHz QPO and the pulse phase shift are all related to each other is currently unknown. It is important to highlight that pulsations are seen in J1900 only in the island/extreme-island (hard) state<sup>4</sup> whereas they disappear in the banana branch (soft-state) except during the aforementioned flare that marked the onset of intermittency ([Galloway et al. 2007](#); [Altamirano & Casella 2008](#)). This could indicate that there is a link between the presence of pulsations and the spectral state of the source.

Another peculiar behavior of J1900 is that the accretion torques operating on the neutron star decrease exponentially with time ([Patruno 2012](#)). This has been interpreted as evidence for magnetic field burial due to accretion (see [Cumming et al. 2001](#)) that could be responsible for reducing the strength of the neutron star magnetosphere. Intermittency and the decreasing strength of the magnetic field might also be related to the peculiar behavior of the burst oscillations seen in J1900. The source has shown several tens of thermonuclear X-ray bursts but only in one case burst oscillations have appeared ([Watts et al. 2009](#)). Such burst oscillations were detected on April 2, 2009, well beyond the point where the last pulsations were seen. The burst oscillations show the typical drift in their frequency of about 1 Hz, similar to that seen in other bursting non-pulsating X-ray binaries and markedly different than burst oscillations in other AMXPs (see [Galloway et al. 2008b](#); [Watts 2012](#) for reviews). An interesting point here is that the burst oscillations appeared during a burst that occurred during another flare, similar to the one described before, when the source moved to the banana branch. Pulsations were not detected around the time of the

<sup>1</sup> Leiden Observatory, Leiden University, Neils Bohrweg 2, 2333 CA, Leiden, The Netherlands

<sup>2</sup> ASTRON, the Netherlands Institute for Radio Astronomy, Postbu 2, 7900 AA, Dwingeloo, the Netherlands

<sup>3</sup> Anton Pannekoek Institute for Astronomy, University of Amsterdam, Postbus 94249, 1090 GE Amsterdam, The Netherlands

<sup>4</sup> Atoll sources trace out a pattern in the color-color diagram with a curved branch called the banana branch, further divided in the upper and lower banana branch (at the highest intensities) which, at the lowest intensity, connects to the island and extreme island state. ([Hasinger & van der Klis 1989](#); [van Straaten et al. 2003, 2005](#)).

burst.

A poorly explored observational diagnostic in HETE J1900.1–2455, that could help to solve some of these puzzles, is the aperiodic variability of the X-ray lightcurve. Indeed it is known that kHz QPOs and other power spectral frequency components are powerful probes of the accretion flow close to the compact object (where magnetospheric effects could be present). For example, the characteristic frequencies of some of the power spectral components of AMXPs (in particular the highest frequency components) are shifted with respect to other non-pulsating atoll sources by a factor 1.1–1.6, depending on the specific source (van Straaten et al. 2003, 2005; Linares et al. 2005; Bult & van der Klis 2015). It is possible that it is the magnetic field of the neutron star that plays a role in generating these shift and therefore it is interesting to investigate this phenomenon in J1900 too.

In this paper we explore all the *RXTE* data collected on J1900 between June 2005 and December 2011 to look for new signatures that might highlight if the magnetosphere in J1900 is typical as in other AMXPs. In particular we look for kHz QPOs, the frequency correlations between different power spectral components and we link the observations to the behavior of the pulsations.

## 2. X-RAY OBSERVATIONS

We used all the *RXTE* Proportional Counter Array (PCA) data recorded over a baseline of 6 years (2005 June to 2011 December). We refer to Jahoda et al. (2006) for PCA characteristics and *RXTE* absolute timing. For our aperiodic timing analysis we used Event and GoodXenon data, with a resolution of  $2^{-13}$  s and  $2^{-20}$  s, respectively. We rebinned the GoodXenon data to the same resolution as the Event data. For the timing analysis, the photons were extracted from the energy band  $\approx 2$ –16 keV (absolute channels 5–37) which is the one that maximizes the signal to noise (S/N) ratio of the pulsations (Patruno 2012) and, as we verified a-posteriori, gives the optimal S/N also for the aperiodic variability. Power spectra were calculated selecting intervals with lengths of 16 s (for the dynamical power spectra) and 128 s (for all other power spectra).

No background is subtracted and no dead time correction is applied prior to calculating the power spectra. After their calculation, we average and Leahy-normalize them by subtracting a Poissonian (counting) noise level that incorporates dead-time effects as explained in Zhang et al. (1995). We then rms-normalize the power by following van der Klis (1995) and using an average background count-rate calculated by processing Standard-2 data with the FTOOL *pcabackest*. In essence, the final power spectra are such that the square root of the integrated power equals the fractional root-mean-square variability in the signal. The power spectra are averaged per observation (obsID) and inspected by eye and those that show significant power are fitted by using a sum of Lorentzians, whose peak frequency is defined according to the definition of Belloni et al. (2002):

$$\nu_{max} = \nu_0 \sqrt{1 + \frac{1}{4Q^2}} \quad (1)$$

where  $\nu_0$  is the centroid frequency and  $Q$  is the quality factor. This latter is defined as the ratio between  $\nu_0$  and the full-width at half maximum of the QPO. In this paper we define the single trial significance  $\sigma$  of a QPO by dividing the integral power of the QPO with its negative error, as is common

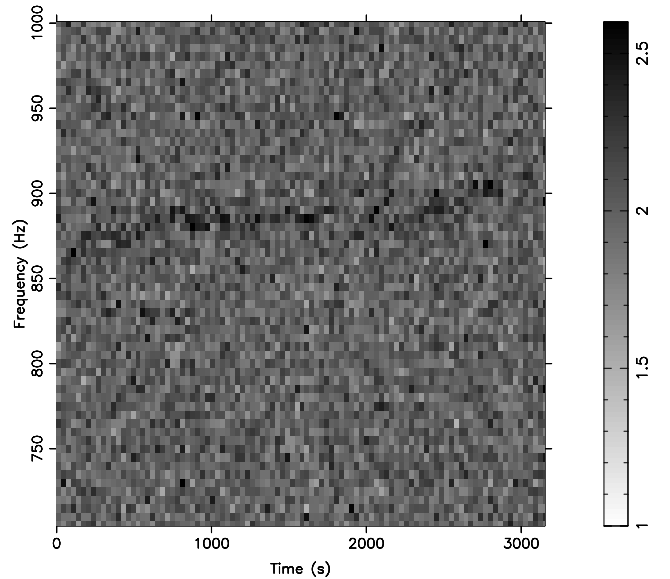


**Figure 1.** Dynamical power spectrum of HETE J1900.1–2455 for the ObsId 91015-01-06-00. This is the observations where the first flare is seen and when the pulses are observed to drift by about 0.5 cycles in  $\approx 3000$  s. At the same time the kHz QPO moves from  $\sim 850$  to  $\sim 900$  Hz.

practice in aperiodic timing studies. The errors on the integral power are determined by varying the minimum  $\chi^2$  such that  $\Delta\chi^2 = 1$ .

To increase the signal-to-noise (S/N) ratio of the broader power spectral features and investigate correlations between them, we then group the observations in such a way that each group contains consecutive observations close in time and in color. When grouping, we allow for a variation of a few percent in color, to guarantee that no spectral transition occurs in each group. Since J1900 has been sparsely monitored, with gaps in consecutive data reaching several days/tens of days, sometimes we use single obsIDs (that we still label as “groups” to keep a uniform nomenclature, see group 3 and 8 in Table 1). We also tried to select groups by choosing observations close in soft and hard colors, regardless of their observing time. However, this grouping scheme does not lead to a better S/N of the different power spectral components, which are often blurred together. This leaves us with a total of 62 groups.

We use the Standard 2 mode data (16 s time resolution) to calculate the aforementioned X-ray colors and intensity. Hard and soft colors are defined, respectively, as the 9.7–16.0 keV/6.0–9.7 keV and the 3.5–6.0 keV/2.0–3.5 keV count rate ratios, whereas the intensity is extracted in the 2–16 keV band. The energy/channel conversion is done by using the *pca\_e2c\_e05v02* table provided by the *RXTE* team. The colors and intensity are calculated after subtracting the background and correcting for dead-time and are normalized to the Crab Nebula values to account for gain changes among the different PCUs that compose the PCA instrument (see Kuulkers et al. 1994; van Straaten et al. 2003).

Finally, when considering the pulse phase drift that occurred at the time of the first flare, we generate the pulsations by following the procedure explained in Patruno (2012). In short, we fold the photon time of arrivals with the orbital and spin frequency parameters of J1900. The only difference here is that we introduce an energy selection for the photons to study the pulse phase energy dependence. We define a soft and a hard band, with absolute channels 5–23 ( $\approx 2$ –9 keV)

and 24–39 ( $\approx$  9–17 keV), respectively. To partially compensate for the loss in S/N due to the energy band selection, we fold the data in segments of 500 s instead of the 300 s chosen by [Patruno \(2012\)](#). The pulsations are considered significant if the ratio between their amplitude and their statistical error is larger than  $3\sigma$ .

### 3. RESULTS

#### 3.1. Aperiodic Variability

We begin by discussing the presence of kHz QPOs in our power spectra, with the results of our analysis presented per observation (obsID). We do this because we want to see if there is a link between the presence of kHz QPOs and the presence of pulsations. Since pulsations appear and disappear on a timescales as short as few minutes, we cannot use the grouped data (which will be used later to look for correlations among the different power spectral components). We detect several kHz QPOs in different observations that can be clearly classified in two categories. The first comprises six observations in which one single kHz QPO is detected (including the 882 Hz QPO previously reported by [Kaaret et al. 2006](#)) with a peak frequency always between  $\approx$ 780 and 900 Hz. The QPO frequency  $\nu_{max}$  is seen to quickly drift by several tens of Hz during some observations (see for example the dynamical power spectrum in [Figure 1](#)). This QPO is seen in the lower left banana state (i.e., the soft state, see [Figure 2](#)) and it is reminiscent of other kHz QPOs seen in atoll sources ([van der Klis 2006](#)). The kHz QPOs are detected with a significance (single trial) between  $3.1$  and  $8\sigma$ . No evidence for any other kHz QPO with frequencies between 100 Hz and the Nyquist frequency is seen in these six observations. We also detect a 883 Hz QPO seen in the island state (with a significance of  $4.1\sigma$ ) in the obsID 92049-01-44-00.

Another observation taken in the island state (ObsID 91015-01-06-02) and recorded four days since the onset of intermittency, shows also a possible kHz QPOs with frequency of  $\approx$  720 Hz, although the significance of the detection is low ( $3.2\sigma$ ). No pulsations were detected in this observation. Given the low significance of the feature we consider the QPO detection as tentative and will not discuss it any further. The second category of QPOs is composed by a kHz QPO with a frequency of  $\approx$  400–500 Hz which appears sometimes in pair with a low frequency (and low Q) feature at around 100–200 Hz during the island state (see an example in [Figure 3](#)).

If these are indeed twin kHz QPOs pairs, then the difference  $\Delta\nu$  between the lower and upper kHz QPO frequency varies between 260 and 380 Hz. However, atoll sources very often show a feature around 100–200 Hz which is called the hecto-Hertz QPO, and we consider it more likely that this is what we are observing in J1900 (see further discussion below). The hHz QPO has the characteristic of having a frequency relatively constant and to be uncorrelated with the other characteristic frequencies seen in the power spectra (see e.g., [van Straaten et al. 2005](#)). In [Figure 4](#) and [5](#) we show the lightcurve of J1900 along with the observations where the different QPOs were detected.

The color-color and hardness-intensity diagram of J1900 (shown in [Figure 2](#)) exhibit a typical atoll source behavior, with the source that spends most of its time in the extreme island state and banana branch at higher luminosity. Based on our previous analysis reported in [Patruno \(2012\)](#), we highlighted all observations where pulsations were detected. We also highlight observations where the 800–900 Hz QPO is de-

tected (red squared) plus those observations with the 400–500 Hz QPO (purple triangles).

We now focus on all the different power-spectral components observed in J1900. Since these components are usually broad we grouped the data as explained in [Section 2](#) to increase the S/N ratio. To better investigate the origin of the kHz QPOs as well as the different power spectral components we fit a multi-Lorentzian empirical model to determine the temporal evolution of the different characteristic frequencies. We name the different power spectral components by following the work of [van Straaten et al. \(2003, 2005\)](#). In brief, power spectra are usually composed by the following Lorentzians ( $L$ ): a low-frequency break ( $L_b$ ), a second break that often appears at high luminosity ( $L_{b2}$ ), the hump ( $L_h$ ), the hecto-Hz QPO ( $L_{hHz}$ ), the low-frequency QPO ( $L_{LF}$ ), a low frequency component ( $L_{low}$ ) which is a possible manifestation of the lower kHz QPO, the lower kHz QPO ( $L_l$ ) and the upper kHz QPO ( $L_u$ ). We anticipate that we do not see all these features in J1900 but we need usually 3 to 4 Lorentzians to obtain a good fit to our power-spectra. In particular, we do not see  $L_{LF}$  and  $L_l$ .

We begin by identifying the low frequency components in each power spectrum, namely  $L_b$ ,  $L_{b2}$  and  $L_h$ . The break and the hump characteristic frequencies are indeed known to follow the so-called WK correlation ([Wijnands & van der Klis 1999](#)). These frequencies measured in J1900 match with great accuracy the known correlation for other atoll sources (see [Figure 6](#)). This means that our identification of those components in the power spectra of J1900 is correct.

We then proceed by looking at the correlations between the upper kHz QPO ( $L_u$ ) and the other characteristic frequencies in the power spectra (namely  $L_b$ ,  $L_h$ ,  $L_{hHz}$  and  $L_{low}$ ). The results are shown in [Figure 7](#), where we display only data points which have an error on  $L_u$  of less than 50 Hz, since larger errors are not particularly constraining. This leave us with 12 groups out of a total of 62 groups considered in this work (see [Table 1](#)).

The data of J1900 clearly suggest that this source behaves as a non-pulsating atoll source, even when pulsations are detected (see [Figure 7](#) where we show the data with pulsations in red and without as black). Some data points are not very constraining since the characteristic frequencies are located towards the lower end of the observed range, where the error bars on all data points are large and the measurements of atoll sources and AMXPs overlap substantially. However, there are data points (some of which were collected in the initial 22 days when the source was a persistent pulsator) that clearly show no shift in characteristic frequencies between J1900 and non-pulsating atoll sources. Second, the relatively constant frequency of the 100–200 Hz feature in [Figure 7](#), along with its low Q value, suggests that indeed we are observing the hHz QPO and we thus have no detection of a lower kHz QPO in J1900 (see [Table 2](#) for a summary of all fitted components).

Finally, we looked for the parallel-track phenomenon, which is seen in several atoll sources (see [van der Klis 2001](#) and [van der Klis 2006](#) for a review). When plotting the upper kHz QPO frequency versus the average 2–16 keV luminosity we see a clear single correlation with no parallel tracks. However, we caution that the number of measurements is relatively small and therefore we cannot firmly conclude that the parallel track phenomenon does not occur in J1900.

#### 3.2. Pulsations

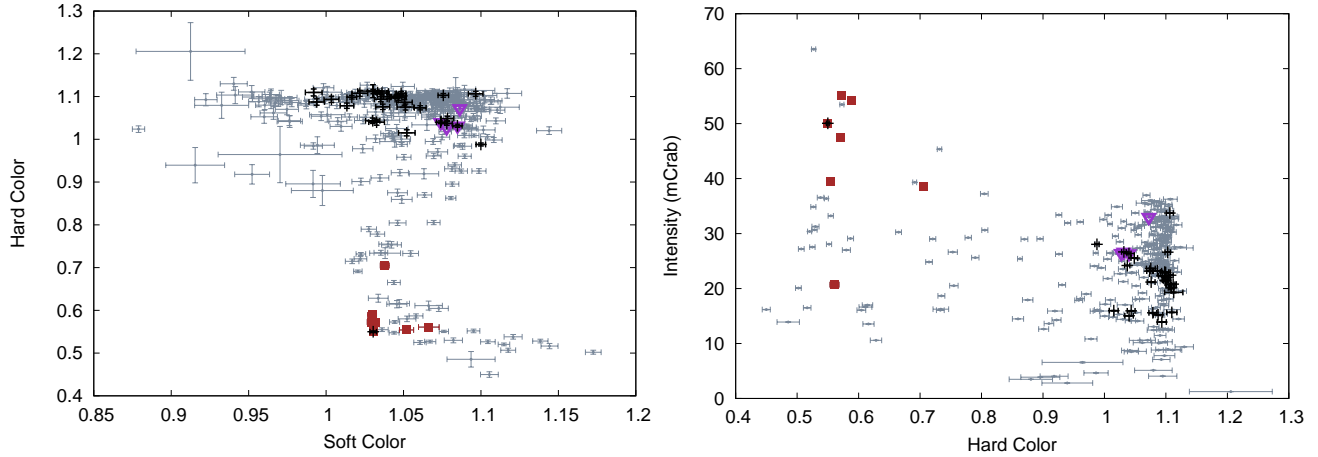


**Figure 2.** Color-color diagram (left panel) and hardness-intensity diagram (right panel) for all the data available for HETE J1900.1-2455 averaged per ObsID and selected such that the intensity is larger than at least 1 mCrab. The red squares are points where the 800–900 kHz QPO is detected. The purple open triangles identify the observations where the 400–500 kHz QPO is observed. The black circles are points where pulsations are seen.

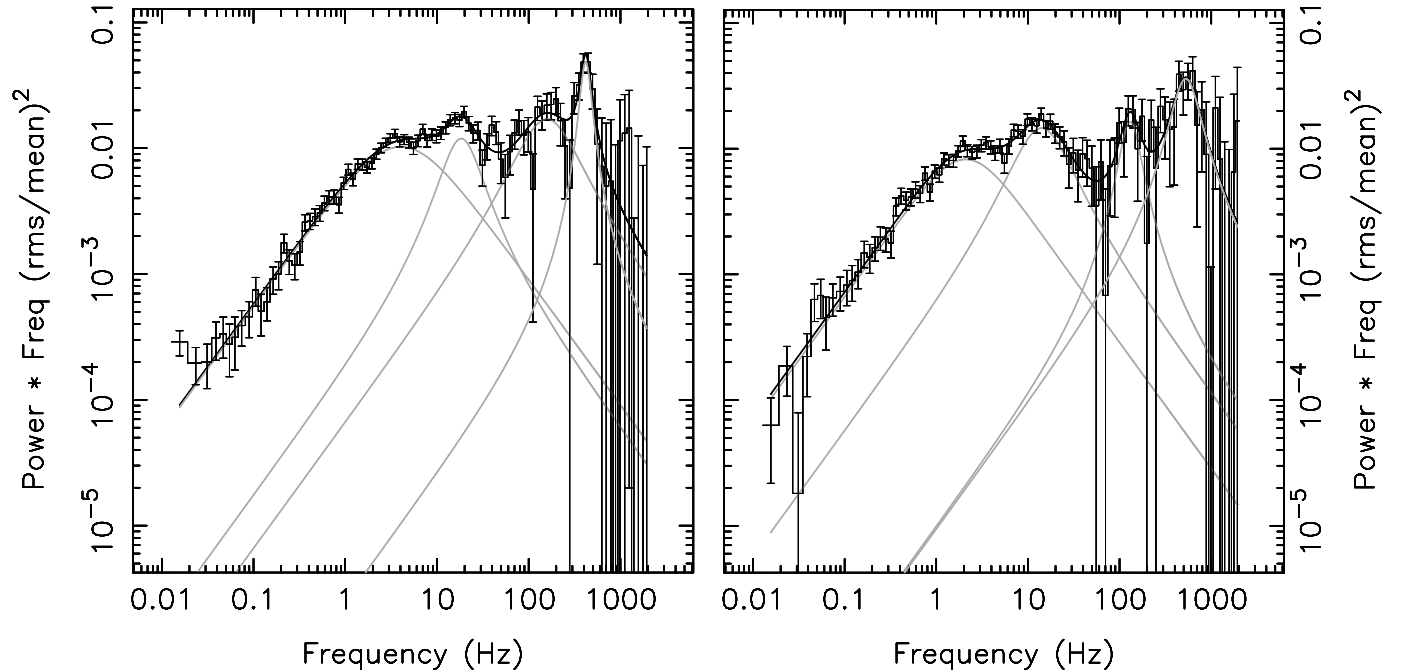


**Figure 3.** Power density spectra of the observations 91015-01-04-04 (left) and 91057-01-04-00 (right). In the plots it's evident the new detected kHz QPO. The frequency of the QPO centroid shifted from  $\sim 420$  Hz (left panel) to  $\sim 510$  Hz (right panel) with the first flare occurring in between these two observations.

We now turn our attention to the drifting pulse episode reported by [Patruno \(2012\)](#) and observed at the time of the first flare. The first striking point to make is that the occurrence of the pulse phase drift happens in coincidence with the beginning of the *RXTE* observation. The timescale for the pulsations to drift by  $\approx 1$  cycle is roughly 6 ks – i.e., about twice the length of the observation (where the pulses are seen to drift by  $\approx 0.5$  cycles). This sets an absolute upper limit to the duration of the drift. The length of the flaring episode is ill constrained on these timescales, since the preceding and following *RXTE* observations (when the source was not in the flare) were taken about 2 days apart (each). Therefore it seems a remarkable (and very unlikely) coincidence that the pulse phases drift by 0.5 cycles exactly when the *RXTE* observation takes place. Indeed if the drift is a unique event that occurs only once during the flare, then it should last no more than  $\approx 6$  ks. But the flar-

ing duration can be anything between 3 ks and 4 days. If the flare has lasted for only  $\approx 6$  ks, then we have a probability of less than 2% to observe, by coincidence, the flare at the right moment with *RXTE*.

To further investigate this phenomenon, we first look at the pulse fractional amplitudes (sinusoidal semi-amplitude). All observations show a relatively constant pulsed fraction (in the 2–16 keV band) at around 2% with no clear trend and/or variation over time. The fractional amplitudes in the  $\approx 2 - 9$  keV soft band ( $\approx 1.5 - 2\%$ ) are about half those in the 9 – 17 keV hard energy band ( $\approx 3 - 4\%$ ). When looking at the pulse phases, the hard band pulses arrive slightly earlier than those in the soft band. The trend of the hard band pulse phases appears also slightly different than the soft pulses, with the former that seem to drift more quickly in the beginning and then reaching a maximum, while the soft pulses keep drifting

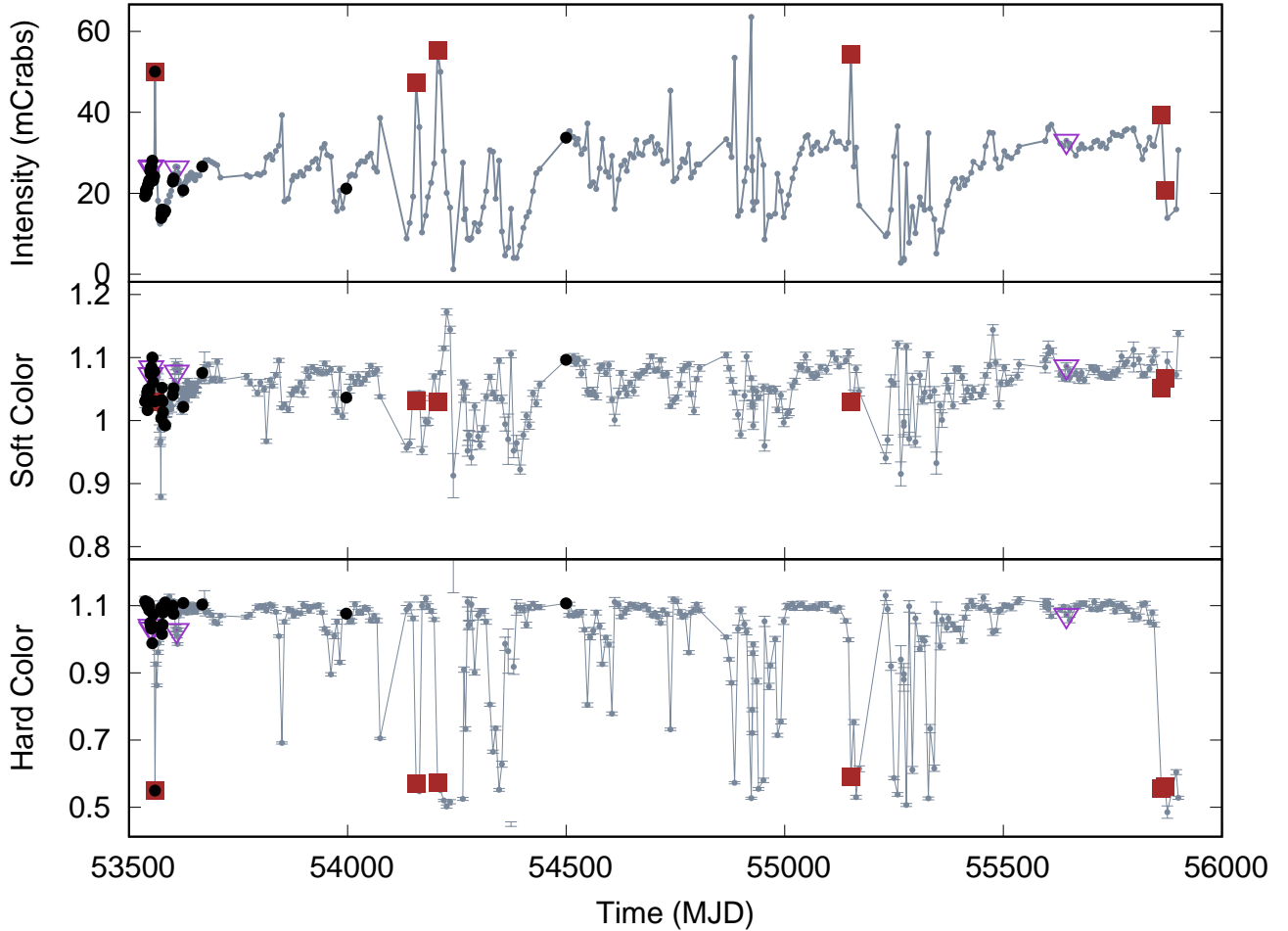


**Figure 4.** The 2–16 keV lightcurve (top panel), soft color (middle panel) and hard color (bottom panel) for all observations recorded by *RXTE* from 2005 to 2011. Observations with pulsations are marked with black circles, the ones with the 800-900 kHz QPO with red squares and those with the 400-500 kHz QPO are identified by open purple triangles.

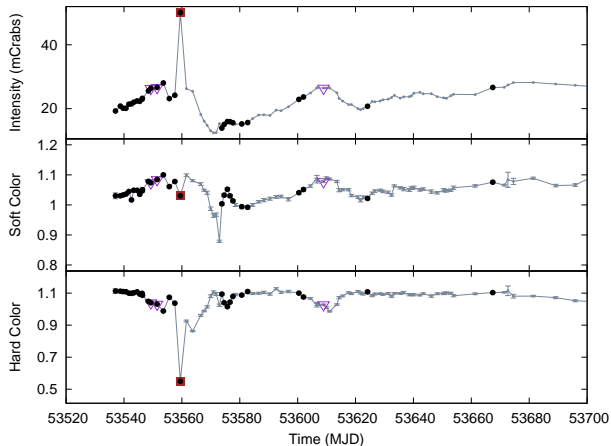


**Figure 5.** A zoom in of the lightcurve in Figure 4 to better display the initial part of the outburst.

at an approximately constant rate.

#### 4. DISCUSSION

We have used all available *RXTE* data of the AMXP HETE J1900.1–2455 to investigate its periodic and aperiodic variability properties. HETE J1900.1–2455 shows three peculiar

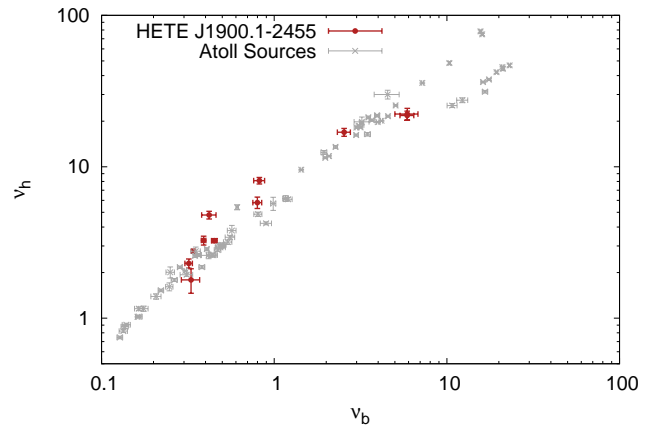


**Figure 6.** WK relation for HETE J1900.1-2455 (red points) over-plotted on the other Atoll sources (gray points, from [van Straaten et al. 2005](#)).

phenomena, namely it has:

1. the break and hump characteristic frequencies which scale with the upper kHz QPO frequency as non-pulsating atoll sources rather than AMXPs;
2. the highest upper kHz QPO frequency ever observed in

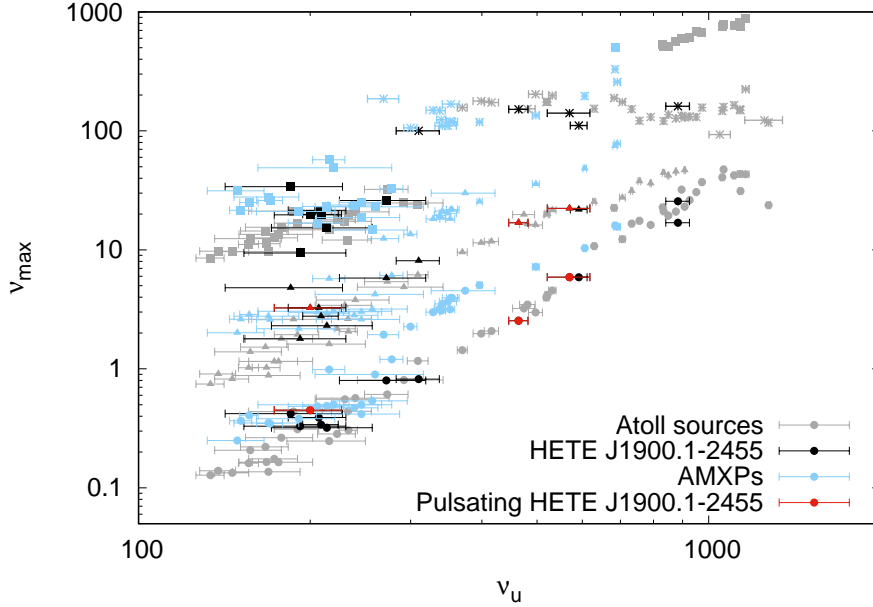


**Figure 7.** Characteristic frequency of the break  $L_b$  (circles), hump  $L_h$  (triangles), hecto-Hz  $L_{hHZ}$  (asterisks), and  $L_{low}$  (squares) versus the upper kHz QPO frequency. The light gray points are atoll sources whereas the light blue points are AMXPs (both data-sets are taken from van Straaten et al. 2005). The black and red points are new measurements done for HETE J1900.1–2455, with data showing pulsations (red) and no pulsations (black). All data with pulsations refer to the initial 22 days of the outburst.

an accreting pulsar ( $\approx 900$  Hz);

3. the largest pulse phase jump of any AMXP ( $\approx 0.6$ – $0.7$  cycles) with the pulse phases drifting by  $\approx 0.5$  cycles in about 3 ks.

It is therefore interesting to ask whether these peculiar phenomena are related to each other and whether they might provide further insight on the physics operating in the inner regions of the accreting neutron star.

The shift in frequencies between power spectral components of other AMXPs and non-pulsating atoll sources (van Straaten et al. 2005) provides a powerful tool to probe the intermittent behavior of J1900. Indeed it is possible that these shifts are related in some way to the presence of a dynamically important magnetosphere in AMXPs. This would seem a natural direction to follow when trying to build a physical interpretation of the data. It is important to stress that when looking at these shifts there are exceptions to the rule. For example, a somewhat smaller shift ( $\approx 1.17$ ) was observed in the non-pulsating atoll source 4U 1820–30 (Altamirano et al. 2005). Another exception is the AMXP IGR J17511–3057, where the shift factor was varying over time and required an offset of about 2 for most observations (Kalamkar et al. 2011). However, we stress that all AMXPs, until now, have been observed with these shifts. We also note that the upper kHz QPO frequencies seen in AMXPs are shifted to lower values with respect to other atoll sources, which is expected if the upper kHz QPO is related to the Keplerian frequency of the inner accretion disk. The inner disk boundary in AMXPs is indeed regulated by the neutron star magnetic field strength that pushes it further out than in non-magnetized neutron-stars. Since all AMXPs show these shifts, it is clear that a magnetosphere is the primary candidate to explain the aperiodic variability phenomenology.

In HETE J1900.1–2455 the scaling of the characteristic frequencies matches very well those of other non-pulsating atoll

sources, both when the source is observed pulsating persistently and when it turns into a non-pulsating source. Therefore what is observed in J1900 argues in favor of a relatively weak magnetosphere that is unable to shift the upper kHz frequency to lower values. The behavior of the other power spectral components of J1900 also closely follows those of other atoll sources, with the caveat that several power spectral components appear slightly shifted in color classification. For example, we see a  $\approx 883$  Hz QPO during the island state, whereas these are usually observed in the lower left banana branch. We also see the hHz QPO in the extreme island state rather than the island state. This anomaly is, however, not unique to J1900 since some atoll sources have shown a similar behavior (e.g., van Straaten et al. 2003; Migliari et al. 2003) as well as an AMXP (Kalamkar et al. 2011).

The second piece of evidence for the presence of a weak magnetosphere comes from the very high frequency QPO observed to reach values of  $\approx 900$  Hz. If this is interpreted as a Keplerian frequency (van der Klis 2000), then this would correspond to a radius of 17–20 km for a neutron star mass of 1.4–2.0  $M_{\odot}$ . If we calculate the magnetosphere radius from the usual expression that equates the ram pressure in the disk to the magnetic pressure of the magnetosphere, then:

$$r_M = \left( \frac{\mu^4}{2GM\dot{M}^2} \right)^{1/7} \quad (2)$$

with  $\mu = BR^3$  the star’s magnetic moment,  $M$  the neutron star’s mass and  $R$  its radius. The actual location of the transition to magnetically dominated flow is, however, more uncertain than this, and a factor  $\xi \approx 0.1 - 1$  is used to parametrize the uncertainties in the physical model (Ghosh & Lamb 1979; Psaltis & Chakrabarty 1999). If we set  $r_M = 17$ – $20$  km and use  $\xi = 1$  for simplicity, then the inferred strength of the magnetic field is of the order of 7– $10 \times 10^7$  G, in line with what was estimated by Patruno (2012) based on the accretion torques

behavior (but again we caution that a lower  $\xi$  would increase  $B$ ).

A third piece of evidence for a weak magnetic field comes from the behavior of the pulsations. The pulse phase drift is anomalous because the probability of observing it by pure chance, given the spacing between consecutive *RXTE* observations of  $\approx 2$  days, is extremely small, less than 2%. This suggests that the 3–6 ks timescale of the drift does not correspond to the total duration of the phenomenon which is very likely much larger than that. The fact that during the drift there is very little variation in pulsed fractional amplitude strongly argues against a small hot spot (drifting in latitude) on the neutron star surface. Indeed, although the amplitude of the pulsations has a complex dependence on a number of physical parameters like the hot spot size, location on the surface, temperature differential etc. (see e.g., [Poutanen & Beloborodov 2006](#)), the small amplitude of the pulsations and the lack of amplitude variability argue in favor of a very large hot spot so that the fraction of neutron star surface irradiating pulsed X-rays remains roughly constant over time. The drift in phase might indicate that the centroid of the emitting region is quickly drifting, possibly because of a reconfiguration of the magnetic field, so that it is the average centroid of the hot spot that quickly moves over time rather than a small size hot spot. If this is the correct explanation, this would again suggest that the magnetosphere in HETE J1900.1–2455 is very weak so that only part of the accretion flow is channeled and/or confined by the magnetic field lines. Finally, the origin of the drift itself remains enigmatic. However, whatever mechanism is responsible for the drift, it must be related to some anomaly in the magnetosphere since it involves the channeling of gas from the disk to the magnetic poles.

AP acknowledges support from a NWO (Netherlands Organization for Scientific Research) Vidi fellowship. RW is

supported by an NWO Top grant, module 1.

## REFERENCES

- Altamirano, D., & Casella, P. 2008, in American Institute of Physics Conference Series, Vol. 1068, American Institute of Physics Conference Series, ed. R. Wijnands, D. Altamirano, P. Soleri, N. Degenaar, N. Rea, P. Casella, A. Patruno, & M. Linares, 63–66
- Altamirano, D., van der Klis, M., Méndez, M., et al. 2005, *ApJ*, 633, 358
- Belloni, T., Psaltis, D., & van der Klis, M. 2002, *ApJ*, 572, 392
- Bult, P., & van der Klis, M. 2015, *ApJ*, 806, 90
- Cumming, A., Zweibel, E., & Bildsten, L. 2001, *ApJ*, 557, 958
- Degenaar, N., Ootes, L. S., Reynolds, M. T., Wijnands, R., & Page, D. 2017, *MNRAS*, 465, L10
- Galloway, D. K., Morgan, E. H., & Chakrabarty, D. 2008a, in AIPC Series, Vol. 1068, A Decade of Accreting Millisecond X-Ray Pulsars, ed. R. Wijnands, D. Altamirano, P. Soleri, N. Degenaar, N. Rea, P. Casella, A. Patruno, & M. Linares, 55–62
- Galloway, D. K., Morgan, E. H., Krauss, M. I., Kaaret, P., & Chakrabarty, D. 2007, *ApJ*, 654, L73
- Galloway, D. K., Muno, M. P., Hartman, J. M., Psaltis, D., & Chakrabarty, D. 2008b, *ApJS*, 179, 360
- Ghosh, P., & Lamb, F. K. 1979, *ApJ*, 234, 296
- Hasinger, G., & van der Klis, M. 1989, *A&A*, 225, 79
- Jahoda, K., Markwardt, C. B., Radeva, Y., et al. 2006, *ApJS*, 163, 401
- Kaaret, P., Morgan, E. H., Vanderspek, R., & Tomsick, J. A. 2006, *ApJ*, 638, 963
- Kalamkar, M., Altamirano, D., & van der Klis, M. 2011, *ApJ*, 729, 9
- Kuulkers, E., van der Klis, M., Oosterbroek, T., et al. 1994, *A&A*, 289, 795
- Linares, M., van der Klis, M., Altamirano, D., & Markwardt, C. B. 2005, *ApJ*, 634, 1250
- Migliari, S., van der Klis, M., & Fender, R. P. 2003, *MNRAS*, 345, L35
- Papitto, A., D’Ai, A., Di Salvo, T., et al. 2013, *MNRAS*, 429, 3411
- Patruno, A. 2012, *ApJL*, in press, arXiv:100
- Patruno, A., & Watts, A. L. 2012, ArXiv e-prints, arXiv:1206.2727
- Poutanen, J., & Beloborodov, A. M. 2006, *MNRAS*, 373, 836
- Psaltis, D., & Chakrabarty, D. 1999, *ApJ*, 521, 332
- van der Klis, M. 1995, in *The Lives of the Neutron Stars*, ed. M. A. Alpar, U. Kiziloglu, & J. van Paradijs, 301–+
- van der Klis, M. 2000, *ARA&A*, 38, 717
- . 2001, *ApJ*, 561, 943
- . 2006, *Rapid X-ray Variability (Compact stellar X-ray sources)*, 39–112
- van Straaten, S., van der Klis, M., & Méndez, M. 2003, *ApJ*, 596, 1155
- van Straaten, S., van der Klis, M., & Wijnands, R. 2005, *ApJ*, 619, 455
- Vanderspek, R., Morgan, E., Crew, G., Graziani, C., & Suzuki, M. 2005, *ATel*, 516, 1
- Watts, A. L. 2012, *ARA&A*, 50, 609
- Watts, A. L., Altamirano, D., Linares, M., et al. 2009, *ApJ*, 698, L174
- Wijnands, R., & van der Klis, M. 1999, *ApJ*, 514, 939
- Zhang, W., Jahoda, K., Swank, J. H., Morgan, E. H., & Giles, A. B. 1995, *ApJ*, 449, 930

**Table 1**  
*RXTE* observation IDs of the fit groups

Group	<i>RXTE</i> observation IDs
1	91015-01-03-03, 91015-01-03-04, 91015-01-03-05, 91015-01-03-06
2	91015-01-04-04, 91015-01-04-06, 91015-01-04-07
3	91015-01-05-00
4	91015-01-06-01, 91015-01-06-02, 91015-01-07-00, 91015-01-07-01
5	91059-03-03-01, 91059-03-03-02, 91059-03-03-03, 91059-03-04-00, 91057-01-01-00, 91057-01-01-01
6	91057-01-04-01, 91057-01-04-02, 91057-01-04-03, 91057-01-04-04, 91057-01-05-00, 91057-01-05-01, 91057-01-05-02, 91057-01-05-03, 91057-01-05-04, 91057-01-06-00, 91057-01-06-01, 91057-01-06-02, 91057-01-06-03, 91057-01-06-04, 91057-01-07-00, 91057-01-07-01, 91057-01-07-02, 91057-01-07-03, 91057-01-07-04, 91057-01-08-00, 91057-01-08-01, 91057-01-08-02, 91057-01-08-03, 91057-01-08-04, 91057-01-09-00, 91057-01-09-01, 91057-01-09-03, 91057-01-10-00, 91057-01-10-01, 91057-01-10-02, 91057-01-10-03, 91057-01-11-00, 91057-01-12-00, 91432-01-01-00, 91432-01-01-01G
7	92049-01-01-00, 92049-01-02-00, 92049-01-04-00, 92049-01-05-00
8	92049-01-44-00
9	93030-01-53-00, 93030-01-54-00
10	93030-01-64-00, 93451-01-01-00, 93451-01-02-00, 93451-01-03-00, 93451-01-04-00, 93451-01-05-00, 93451-01-06-00, 93451-01-07-00, 93451-01-08-00, 93451-01-09-00, 94030-01-01-00, 94030-01-02-00
11	94030-01-20-00, 94030-01-21-00, 94030-01-22-00, 94030-01-23-00, 94030-01-24-00, 94030-01-25-00, 94030-01-26-00, 94030-01-27-00, 94030-01-28-00, 94030-01-29-00, 94030-01-30-00, 94030-01-31-00, 94030-01-32-00, 94030-01-34-00, 94030-01-36-00, 94030-01-37-00, 94030-01-38-00, 94030-01-40-00, 94030-01-41-00
12	95030-01-40-00, 95030-01-41-00, 95030-01-42-00, 95030-01-44-00, 95030-01-45-00, 96030-01-01-00, 96030-01-01-01, 96030-01-02-00, 96030-01-02-01, 96030-01-03-00, 96030-01-06-00, 96030-01-07-00, 96030-01-08-00

**Note.** — Subdivision of *RXTE* observation IDs in groups as used in this paper. The groups reported are only those for which we have sufficient S/N to allow a secure identification of the power spectral components, out of a total of 62 groups analyzed.

**Table 2**  
 Characteristic frequencies of the multi-Lorentzian fit for HETE J1900.1–2455

Group	$L_b$ (Hz)	$L_{b2}$ (Hz)	$L_h$ (Hz)	$L_{low}$ (Hz)	$L_{hHz}$ (Hz)	$L_u$ (Hz)
1	$0.451^{0.017}_{-0.014}$	–	$3.25 \pm 0.10$	$19.7^{4.3}_{-4.1}$	–	$200^{27}_{-24}$
2	$2.54^{0.22}_{-0.32}$	–	$16.9^{1.0}_{-1.3}$	–	$152^{15}_{-12}$	$464^{18}_{-24}$
3	$5.9 \pm 0.9$	–	$22.3^{2.0}_{-1.8}$	–	$141^{39}_{-26}$	$570^{49}_{-52}$
4	$5.89^{0.54}_{-0.50}$	–	$21.8^{1.5}_{-1.4}$	–	$111^{19}_{-14}$	$592^{20}_{-30}$
5	$0.42^{0.04}_{-0.03}$	–	$4.80^{0.28}_{-0.26}$	$34 \pm 3$	–	$185^{43}_{-40}$
6	$0.337^{0.008}_{-0.007}$	–	$2.77 \pm 0.07$	$19.9^{1.3}_{-1.4}$	–	$209 \pm 15$
7	$0.33 \pm 0.04$	–	$1.79^{0.33}_{-0.30}$	$9.42^{0.91}_{-0.77}$	–	$192^{39}_{-29}$
8	$25.6^{1.0}_{-0.9}$	$16.9^{9.7}_{-9.8}$	–	–	$161^{29}_{-19}$	$883^{42}_{-36}$
9	$0.83^{0.06}_{-0.05}$	–	$8.1 \pm 0.4$	–	$100^{14}_{-7}$	$310^{26}_{-28}$
10	$0.799^{0.047}_{-0.052}$	–	$5.8^{0.5}_{-0.4}$	$26^{15}_{-10}$	–	$272^{47}_{-39}$
11	$0.319^{0.016}_{-0.015}$	–	$2.3^{0.16}_{-0.14}$	$15.3^{2.8}_{-2.0}$	–	$214^{43}_{-41}$
12	$0.389^{0.012}_{-0.014}$	–	$3.26^{0.22}_{-0.16}$	$21.5^{4.2}_{-2.7}$	–	$207^{24}_{-21}$

**Note.** — Characteristic frequencies ( $\equiv \nu_{\max}$ ) of the Lorentzians used to model the power spectra of HETE J1900.1–2455. The errors are evaluated for  $\Delta\chi^2 = 1.0$ .